Supporting Information

Dysprosium(III) compounds assembled via a versatile ligand incorporating salicylic hydrazide and 8-hydroxyquinolin units: Syntheses, structures and magnetic properties

Li Zhang,[a,d] Vincent Montigaud,[b] Boris Le Guennic,*[b] Peng Zhang*[c] and Jinkui Tang*[a]

[a] State Key Laboratory of Rare Earth Resource Utilization, Changchun Institute of Applied Chemistry, Chinese Academy of Sciences, Changchun 130022, P. R. China
[b] Univ Rennes, CNRS, ISCR (Institut des Sciences Chimiques de Rennes) - UMR 6226, F-35000 Rennes, France

[c] School of Chemistry & Chemical Engineering, Shaanxi Normal University, Xi'an, Shaanxi 710062, P. R. China
[d] Key Laboratory of Synthetic and Natural Functional Molecule Chemistry of the Ministry of Education, College of Chemistry and Materials Science, Northwest University, Xi'an 710069, P. R. China

Corresponding Authors
*E-mail: tang@ciac.ac.cn; boris.leguennic@univ-rennes1.fr.; peng.zhang@snnu.edu.cn

Computational details

The atomic positions were extracted from the X-ray diffraction crystal structures. A calculation is performed on the asymmetric Dy^{III} ion of each dimer while the second Dy^{III} is replaced by a diamagnetic Y^{III} ion. All ab-initio calculations were performed using the State-Averaged Complete Active Space Self-Consistent Field approach with restricted-active-space-state-interaction method (SA-CASSCF/RASSI-SO), as implemented in the MOLCAS quantum-chemistry package (version 8.0).[1] The relativistic effects are treated in two steps on the basis of the Douglas–Kroll Hamiltonian. The scalar terms were included in the basis-set generation and were used to determine the CASSCF wavefunctions and energies.[2] Spin-orbit coupling was then added within the RASSI-SO method, which mixes the calculated CASSCF wavefunctions.[3, 4] The resulting spin-orbit wavefunctions and energies were used to compute the magnetic properties and g-tensors of the ground state multiplet following the pseudospin 1/2 formalism, as implemented in the SINGLE-ANISO routine.[5] The resulting mononuclear fragments are then used to compute the anisotropic exchange interactions between the magnetic centers within the Lines model[6] with the software POLY_ANISO.[7] Cholesky decomposition of the bielectronic integrals was employed to save disk space and to speed up the calculations.[8]

The active space considered in the calculations consisted of the nine 4f electrons of the Dy^{III} ion, spanning the seven 4f orbitals; that is, CAS(9,7)SCF. State-averaged CASSCF calculations were performed for all of the sextets (21 roots), all of the quadruplets (224 roots) and 300 out of the 490 doublets of the Dy^{III} ion. Twenty-one sextets, 128 quadruplets and 107 doublets were mixed through spin–orbit coupling in RASSI-SO. All atoms were described with ANO-RCC basis sets with the following contractions [8s7p4d3f2g1h] for Dy; [7s6p4d2f1g] for Y; [4s3p2d] for the N and O atoms close to the center; [3s2p] for the other N and O atoms; [3s2p] for the C atoms and [2s] for the H atoms.[9,10]

To give more insights on the orientation of the magnetic axis, the molecular electrostatic potential is calculated from the *ab-initio* LOPROP charge analysis[11] *(eq. S1)*.

$$V(r_i) = \sum_i^N \frac{q_i}{|r_i - r|} + \frac{p_i \cdot r_i}{|r_i - r|^3} + \frac{r_i \cdot (Q_i \times r_i)}{|r_i - r|^5} \qquad \textit{(eq. S1)}$$

where q_i, p_i, Q_i are respectively the monopole, dipole and quadrupole moments of the i-th atom. The resulting molecular electrostatic potential is mapped and represented using the home-made **CAMMEL** code (**CA**lculated **M**olecular **M**ultipolar **EL**ectrostatics).[12-14] The potential is drawn on a sphere defined by the user around the central lanthanide ion, for a given state (ground state in this case). For a clearer representation of the potential, the intensity can be directly related to both the color (red = high potential and blue = low potential) and the height of the irregularities.

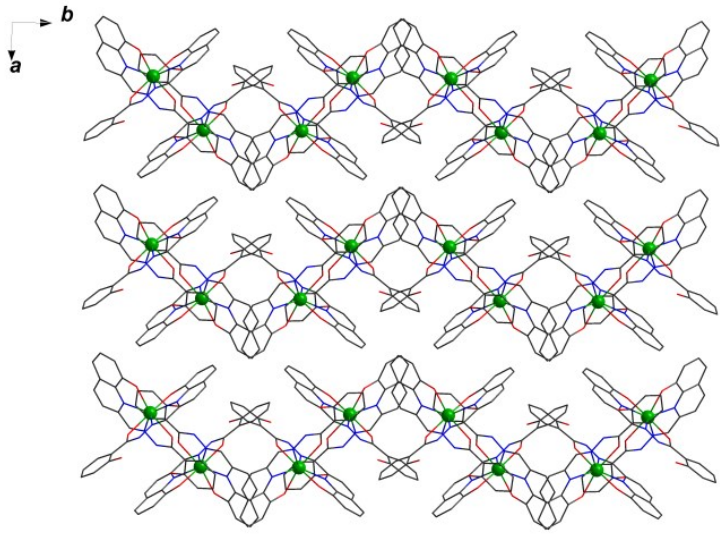

Fig. S1 Perspective view of crystal packing along the crystallographic c-axis in **1**. Color scheme: Green Dy, red O, blue N, black C.

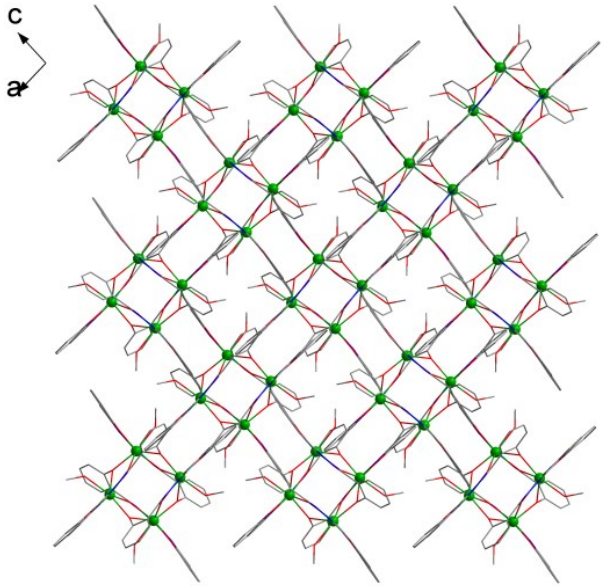

Fig. S2 Packing arrangement along the crystallographic b-axis for complex **4**. Color scheme: Green Dy, red O, blue N, black C.

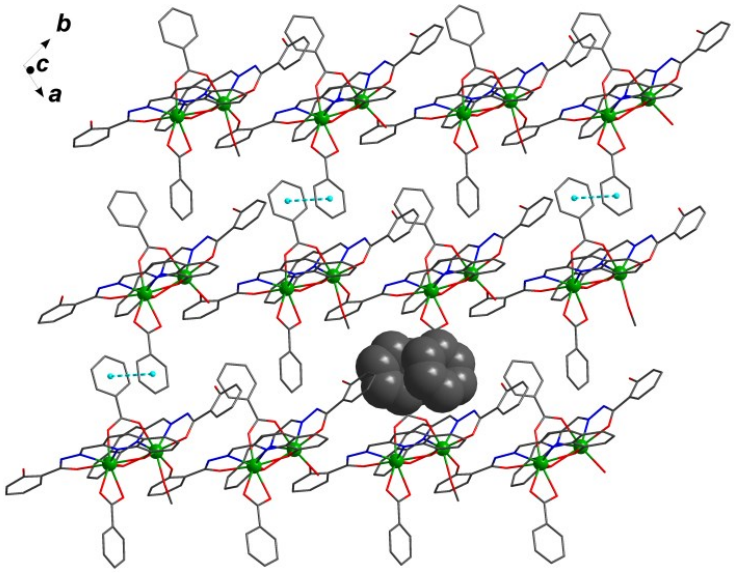

Fig. S3 A small portion of the 2D network of **5** formed by π-π stacking interactions (dashed blue lines).

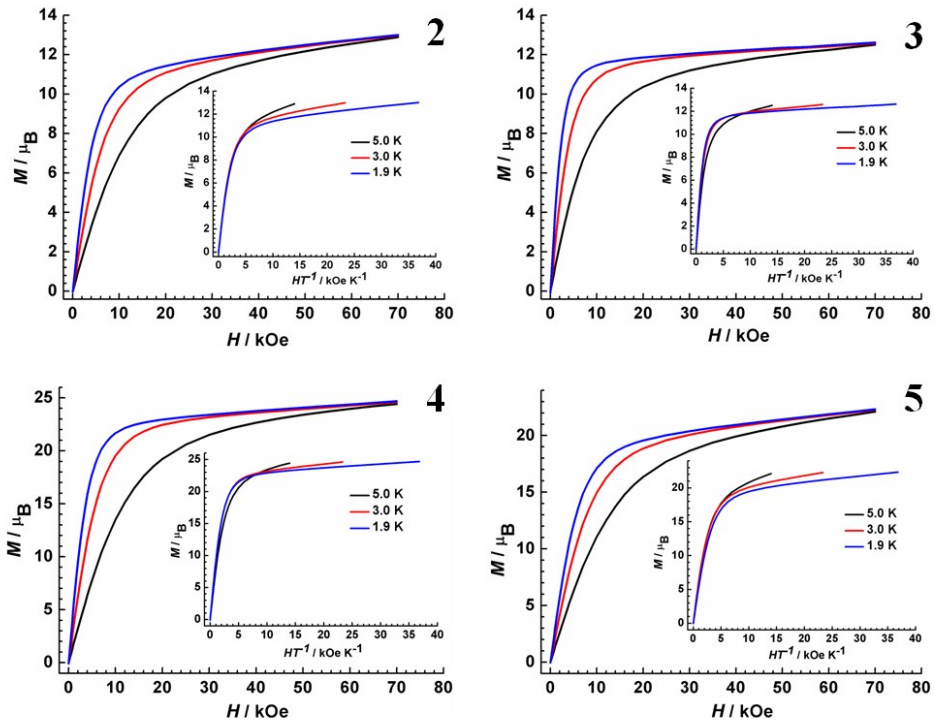

Fig. S4 Field dependences of magnetization in the field range 0-70 kOe and at the range of 1.9-5.0 K. Insets: Plots of the reduced magnetization *M* versus *H*/*T* for **2**-**5**.

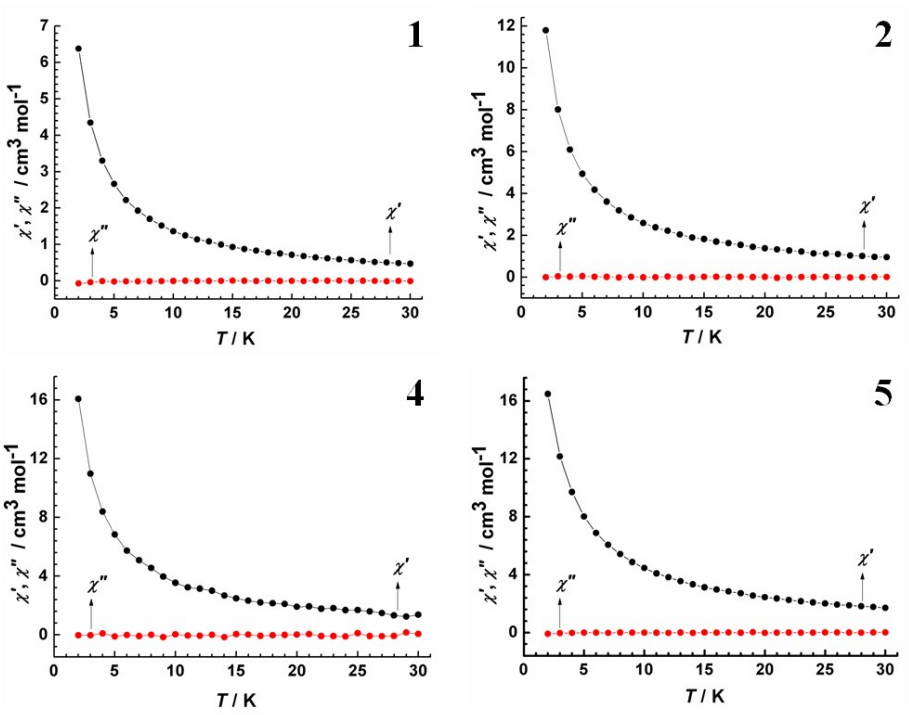

Fig. S5 Temperature dependences of χ' (black) and χ'' (red) of **1**, **2**, **4** and **5** measured at 997 Hz in a zero dc field.

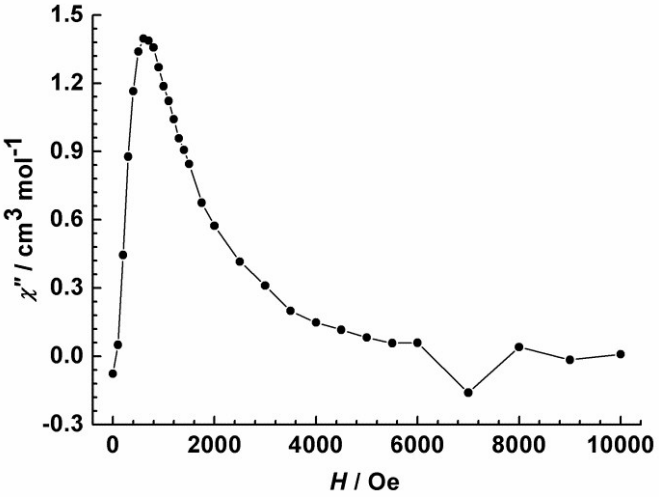

Fig. S6 Dependence of the out-of-phase signal of **1** on applied dc field strength at 1.9 K, 997 Hz.

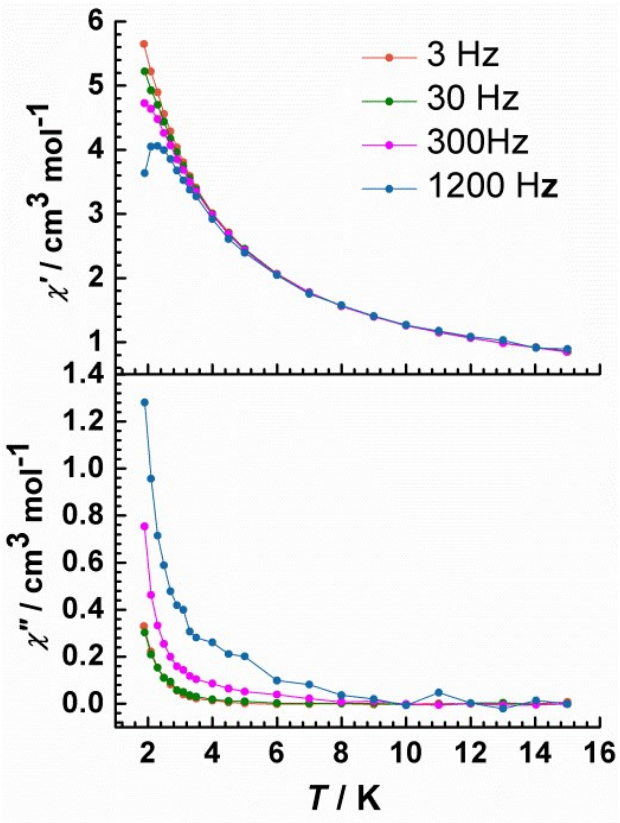

Fig. S7 Temperature dependence of the in-phase (top) and out-of-phase (bottom) ac susceptibility under 600 Oe dc field for **1**.

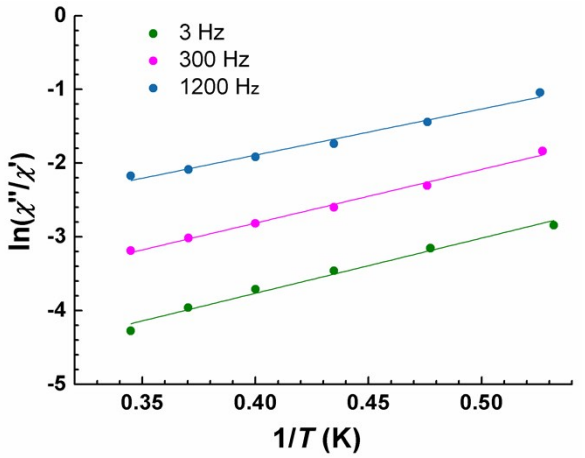

Fig. S8 Plots of natural logarithm of χ''/ χ' *vs.* 1/*T* for **1**. The solid line represents a fit of the results over the range of 3-1200 Hz based on the following relation: $\ln\left(\chi''/\chi'\right)=\ln\left(\omega\tau_0\right)+E_a/k_BT$

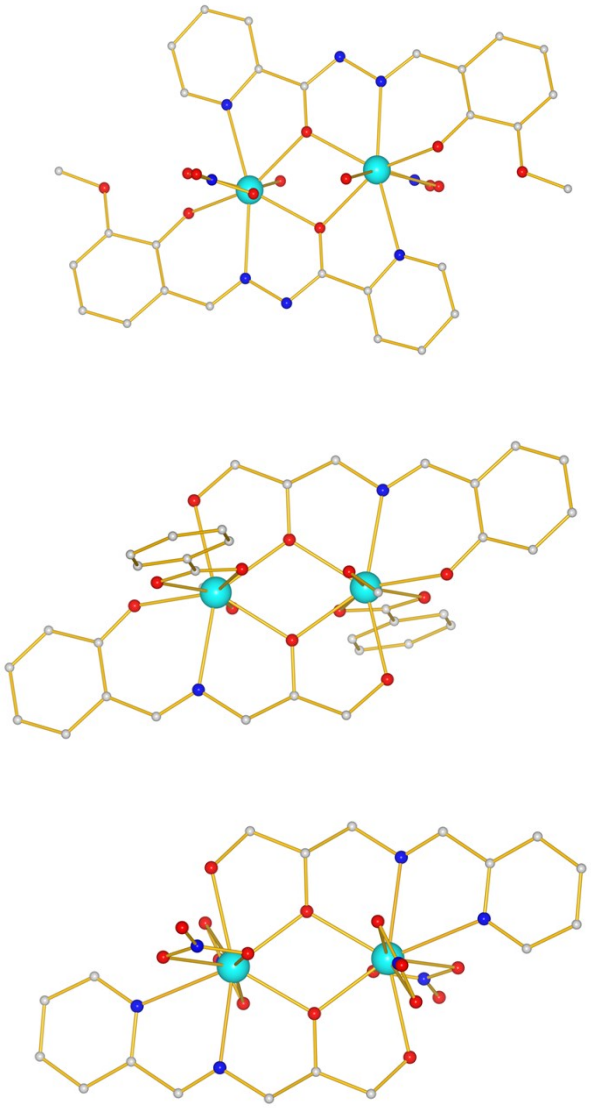

Fig. S9 From top to bottom. The structures of complexes **6**, **7**, **8**, that were reported already in (a) Guo, Y.-N.; Chen, X.-H.; Xue, S.; Tang, J. Modulating Magnetic Dynamics of Three Dy_2 Complexes through Keto-Enol Tautomerism of the o-VanillinPicolinoylhydrazone Ligand.Inorg. Chem. 2011, 50, 9705. (b) Zhang, P.; Zhang, L.; Lin, S.-Y.; Xue, S.; Tang, J. Modulating Magnetic Dynamics of Dy_2 System through the Coordination Geometry and Magnetic Interaction. Inorg. Chem. 2013, 52, 4587. (c) Wang, X., Wang, L.-Y., Wu, S.-Y., Ou, L.-J., Yang, G.-P. Ligand effect of two Dy(III) complexes on single-molecule magnetism, Polyhedron 2020, 184, 114553. (Complex **8** was also reproduced in our group with the crystallographic data: $C_{18}H_{22}Dy_2N_8O_{16}$, M_r = 931.44, Monoclinic, space group $P2_1/c$, a = 9.2453(8), b = 8.1131(7), c = 18.5728(15) Å, α = 90.00, β = 92.2610(10), γ = 90.00°, V = 1392.0(2) Å^3, Z = 2, T = 286(2) K, D_c = 2.222 g cm^{-3}, 2483 reflections collected with 2256 unique (R_{int} = 0.0303), S = 1.058, R_1 = 0.0253 for 2256 reflections with $I > 2\sigma(I)$. The final wR_2 was 0.0636 (all data).)

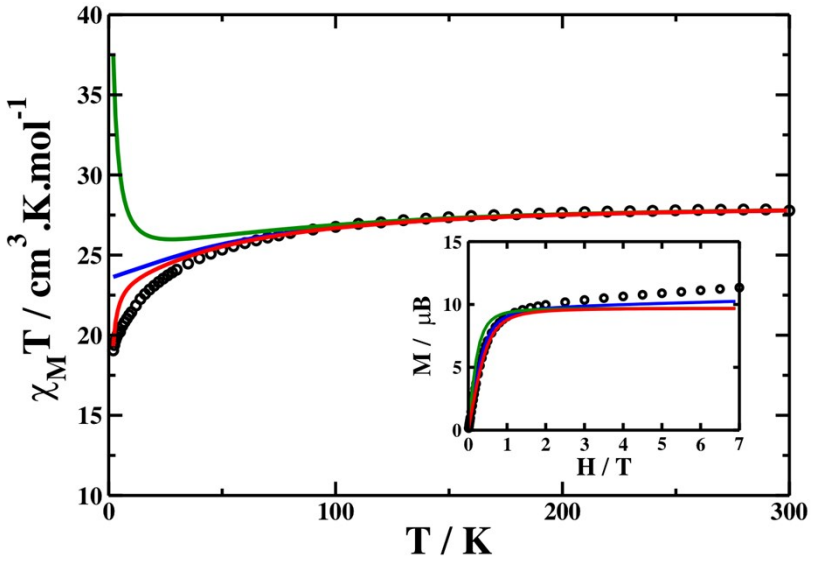

Fig. S10 Thermal evolution of the magnetic susceptibility and evolution of the magnetization with applied magnetic field (inset) for complex ***2***. The experimental values are scaled according to the theoretical value, at 300K (F = 0.872), and represented as dark dots while theoretical values are represented as coloured lines. The blue lines correspond to the overall evolution of the $\chi_M T$ product considering isolated Dy centers (no interactions between them). The green and red curves represent the results obtained for calculations considering respectively only the dipolar interactions and both dipolar and the fitted exchange interactions between the magnetic centers. The best fit of the $\chi_M T$ product was found for J_{ex}= -1.20cm^{-1} (Lines model).

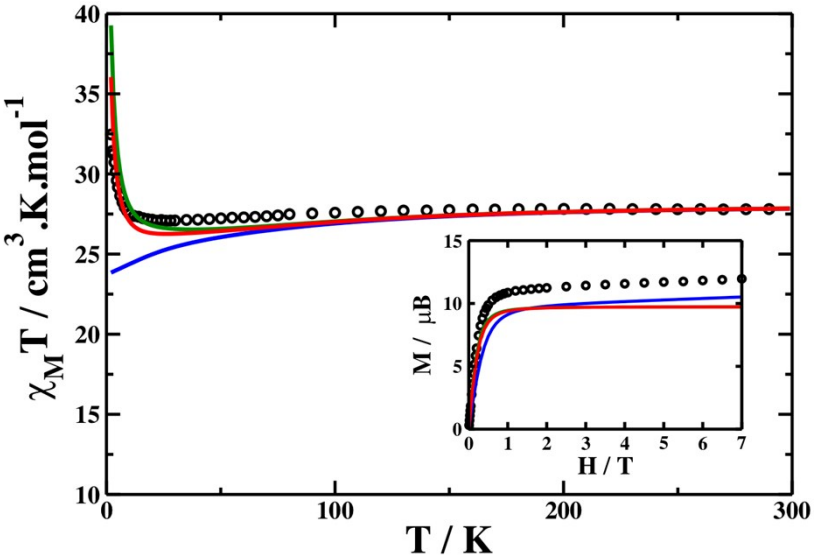

Fig. S11 Thermal evolution of the magnetic susceptibility and evolution of the magnetization with applied magnetic field (inset) for complex **3**. The experimental values are scaled according to the theoretical value, at 300K (F = 0.948), and represented as dark dots while theoretical values are represented as coloured lines. The blue lines correspond to the overall evolution of the $\chi_M T$ product considering isolated Dy centers (no interactions between them). The green and red curves represent the results obtained for calculations considering respectively only the dipolar interactions and both dipolar and the fitted exchange interactions between the magnetic centers. The best fit of the $\chi_M T$ product was found for J_{ex}= -0.29 cm^{-1} (Lines model).

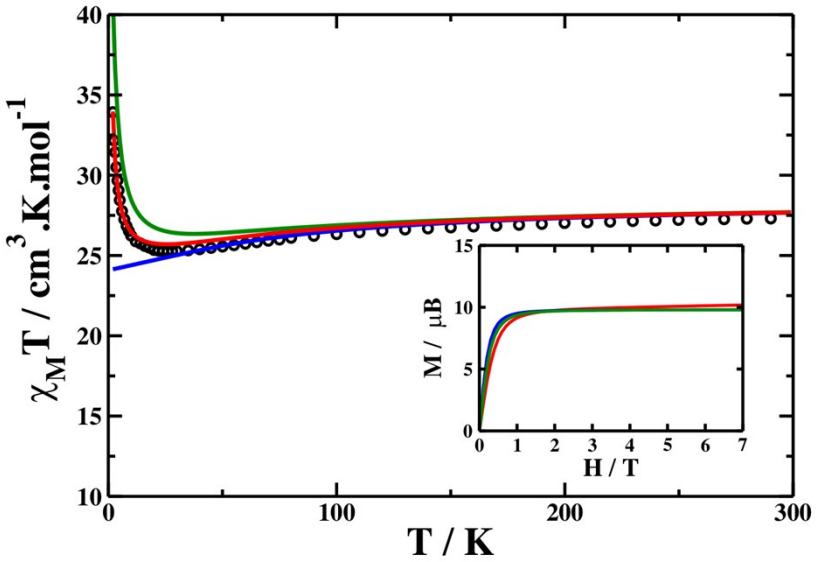

Fig. S12 Thermal evolution of the magnetic susceptibility and evolution of the magnetization with applied magnetic field (inset) for complex **6**. The experimental values are represented as dark dots while theoretical values are represented as coloured lines. The blue lines correspond to the overall evolution of the $\chi_M T$ product considering isolated Dy centers (no interactions between them). The green and red curves represent the results obtained for calculations considering respectively only the dipolar interactions and both dipolar and the fitted exchange interactions between the magnetic centers. The best fit of the $\chi_M T$ product was found for J_{ex}= -0.59 cm^{-1} (Lines model).

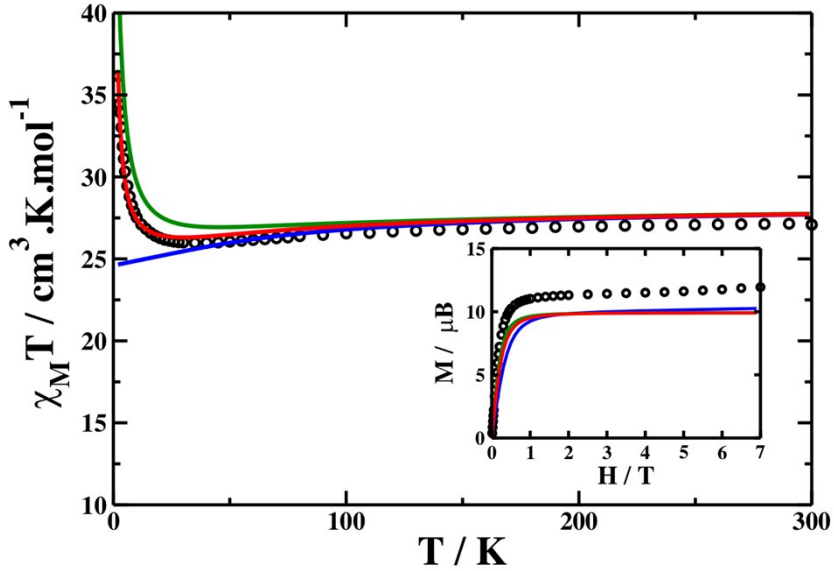

Fig. S13 Thermal evolution of the magnetic susceptibility and evolution of the magnetization with applied magnetic field (inset) for complex **7**. The experimental values are represented as dark dots while theoretical values are represented as coloured lines. The blue lines correspond to the overall evolution of the $\chi_M T$ product considering isolated Dy centers (no interactions between them). The green and red curves represent the results obtained for calculations considering respectively only the dipolar interactions and both dipolar and the fitted exchange interactions between the magnetic centers. The best fit of the $\chi_M T$ product was found for J_{ex} = -0.66 cm^{-1} (Lines model).

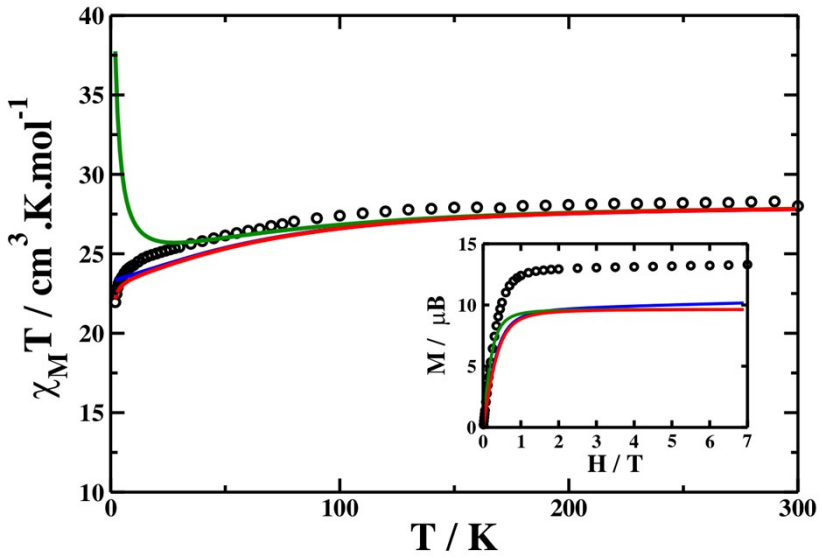

Fig. S14 Thermal evolution of the magnetic susceptibility and evolution of the magnetization with applied magnetic field (inset) for complex **8**. The experimental values are represented as dark dots while theoretical values are represented as coloured lines. The blue lines correspond to the overall evolution of the $\chi_M T$ product considering isolated Dy centers (no interactions between them). The green and red curves represent the results obtained for calculations considering respectively only the dipolar interactions and both dipolar and the fitted exchange interactions between the magnetic centers. The best fit of the $\chi_M T$ product was found for J_{ex} = -1.08 cm^{-1} (Lines model).

Table S1 Crystallographic Data and Structure Refinement Details of Compounds **1**-**5**.

Compound	**1**	**2**	**3**	**4**	**5**
Formula	$C_{35}H_{27}DyN_6O_7$	$C_{53}H_{52}Dy_2N_6O_{15}$	$C_{58}H_{78}Dy_2N_{16}O_{20}$	$C_{74}H_{72}Dy_4N_{12}O_{22}$	$C_{101}H_{83}Dy_4N_{13}O_{25}$
Mr	806.12	1338.00	1644.36	2131.44	2528.80
Crystal system	Monoclinic	Triclinic	Monoclinic	Monoclinic	Triclinic
Space group	$P2_1/c$	P-1	$P2_1/c$	$C2/c$	P-1
T [K]	296(2)	296(2)	296(2)	296(2)	296(2)
a [Å]	12.720(2)	10.6137(10)	16.829(2)	19.5409(19)	14.4228(7)
b [Å]	21.310(4)	10.8593(10)	17.777(2)	21.972(2)	17.5511(9)
c [Å]	12.720(2)	11.3970(11)	12.5849(17)	19.385(2)	20.2386(10)
α [°]	90	78.970(2)	90	90	106.3810(10)
β [°]	109.36	81.792(2)	108.326(2)	93.725(2)	94.9340(10)
γ [°]	90	87.250(2)	90	90	93.7770(10)
V [Å^3]	3252.8(9)	1275.8(2)	3574.1(8)	8305.4(15)	4875.1(4)
Z	4	1	2	4	2
ρ_{calcd} [g cm^{-3}]	1.646	1.741	1.528	1.705	1.723
μ(Mo-Kα) [mm^{-1}]	2.357	2.982	2.153	3.634	3.113
F (000)	1604	664	1660	4160	2488
Reflns collected	17598	7172	21937	25929	25173
Unique reflns	6420	5038	7023	8337	17127
R_{int}	0.0467	0.0236	0.0643	0.0719	0.0457
Parameters /restraints	446 / 0	350 / 26	442 / 36	509 / 16	1304 / 6
GOF	1.017	1.084	1.026	1.050	1.044
R_1 [I > 2σ(I)]	0.0358	0.0380	0.0491	0.0555	0.0524
wR_2 (all data)	0.0853	0.0933	0.1353	0.1668	0.1199

Table S2 Selected bond lengths [Å] and angles [°] for **1**-**5**.

Compound **1**

Dy(1)-O(1)	2.279(3)	Dy(1)-O(5)	2.311(3)	Dy(1)-N(4)	2.437(4)
Dy(1)-O(2)	2.399(3)	Dy(1)-N(1)	2.457(4)	Dy(1)-N(5)	2.473(4)
Dy(1)-O(4)	2.344(3)	Dy(1)-N(2)	2.536(4)		
O(1)-Dy(1)-O(2)	164.77(11)	O(2)-Dy(1)-N(2)	62.64(11)	O(5)-Dy(1)-N(4)	127.38(11)
O(1)-Dy(1)-O(4)	89.63(11)	O(2)-Dy(1)-N(4)	81.72(12)	O(5)-Dy(1)-N(5)	63.56(11)
O(1)-Dy(1)-O(5)	99.27(12)	O(2)-Dy(1)-N(5)	86.57(11)	N(1)-Dy(1)-N(2)	62.23(12)
O(1)-Dy(1)-N(1)	68.05(11)	O(4)-Dy(1)-N(1)	91.25(12)	N(1)-Dy(1)-N(4)	144.34(12)
O(1)-Dy(1)-N(2)	130.06(11)	O(4)-Dy(1)-N(2)	87.11(11)	N(1)-Dy(1)-N(5)	132.85(12)
O(1)-Dy(1)-N(4)	83.25(12)	O(4)-Dy(1)-N(4)	67.03(11)	N(2)-Dy(1)-N(4)	138.75(12)
O(1)-Dy(1)-N(5)	89.07(11)	O(4)-Dy(1)-N(5)	130.76(11)	N(2)-Dy(1)-N(5)	128.62(12)
O(2)-Dy(1)-O(4)	82.25(11)	O(4)-Dy(1)-O(5)	163.65(10)	N(4)-Dy(1)-N(5)	63.94(12)
O(2)-Dy(1)-O(5)	91.84(12)	O(5)-Dy(1)-N(1)	79.56(12)		
O(2)-Dy(1)-N(1)	124.72(11)	O(5)-Dy(1)-N(2)	76.65(11)		

Compound **2**

Dy(1)-O(1)	2.366(4)	Dy(1)-O(1)#1	2.339(4)	Dy(1)-O(6)	2.367(5)
Dy(1)-O(2)	2.291(4)	Dy(1)-Dy(1)#1	3.8013(5)	Dy(1)-N(1)	2.446(4)
Dy(1)-O(4)	2.429(4)	Dy(1)-O(5)	2.383(4)	Dy(1)-N(2)	2.486(5)
O(1)-Dy(1)-O(2)	165.99(13)	O(2)-Dy(1)-O(1)#1	94.28(14)	N(1)-Dy(1)-O(1)#1	134.00(13)
O(1)-Dy(1)-N(1)	66.97(13)	O(2)-Dy(1)-N(1)	126.96(14)	N(2)-Dy(1)-O(1)#1	145.08(15)
O(1)-Dy(1)-N(2)	129.75(14)	O(2)-Dy(1)-N(2)	63.82(14)		
O(1)-Dy(1)-O(1)#1	72.21(14)	N(1)-Dy(1)-N(2)	63.44(15)		
#1 -x+1, -y, -z+1					

Compound **3**

Dy(1)-O(1)	2.399(4)	Dy(1)-O(1)#1	2.371(4)	Dy(1)-N(2)	2.515(5)
Dy(1)-O(2)	2.354(4)	Dy(1)-O(7)	2.389(4)	O(1)-Dy(1)#1	2.371(4)
Dy(1)-O(4)	2.611(5)	Dy(1)-O(8)	2.375(4)	Dy(1)-Dy(1)#1	3.9523(7)
Dy(1)-O(5)	2.520(5)	Dy(1)-N(1)	2.480(4)		
O(1)-Dy(1)-O(2)	164.87(14)	O(2)-Dy(1)-O(1)#1	96.79(14)	N(1)-Dy(1)-O(1)#1	124.25(14)
O(1)-Dy(1)-N(1)	66.04(14)	O(2)-Dy(1)-N(1)	125.73(15)	N(2)-Dy(1)-O(1)#1	142.40(15)
O(1)-Dy(1)-N(2)	128.47(14)	O(2)-Dy(1)-N(2)	63.14(15)		
O(1)-Dy(1)-O(1)#1	68.11(14)	N(1)-Dy(1)-N(2)	62.77(16)		
#1 -x, -y+1, -z+1					

Compound **4**

Dy(1)-O(1)	2.315(7)	Dy(1)-N(1)	2.474(9)	Dy(2)-O(6)	2.288(6)
Dy(1)-O(2)	2.387(6)	Dy(1)-N(2)	2.535(9)	Dy(2)-O(7)	2.389(7)
Dy(1)-O(3)#1	2.286(6)	Dy(2)-O(2)	2.396(6)	Dy(2)-N(4)	2.464(9)
Dy(1)-O(5)#1	2.400(7)	Dy(2)-O(3)	2.357(6)	Dy(2)-N(5)	2.512(10)
Dy(1)-O(6)	2.362(6)	Dy(2)-O(4)	2.298(7)	Dy(1)-Dy(2)	3.9115(7)
Dy(1)-O(8)	2.376(7)	Dy(2)-O(5)	2.388(6)	Dy(1)-Dy(2)#1	3.9134(7)
O(1)-Dy(1)-O(2)	164.2(2)	O(5)#1-Dy(1)-N(2)	136.7(2)	O(3)-Dy(2)-N(5)	120.6(3)
O(1)-Dy(1)-O(5)#1	83.8(2)	O(6)-Dy(1)-O(5)#1	68.9(2)	O(4)-Dy(2)-O(5)	165.1(3)
O(1)-Dy(1)-O(6)	99.7(2)	O(6)-Dy(1)-N(1)	147.4(3)	O(4)-Dy(2)-O(6)	94.6(2)
O(1)-Dy(1)-N(1)	65.6(3)	O(6)-Dy(1)-N(2)	120.9(2)	O(4)-Dy(2)-N(4)	66.3(3)
O(1)-Dy(1)-N(2)	129.1(3)	N(1)-Dy(1)-N(2)	63.7(3)	O(4)-Dy(2)-N(5)	129.3(3)
O(2)-Dy(1)-O(3)#1	99.4(2)	O(2)-Dy(2)-O(3)	68.6(2)	O(5)-Dy(2)-O(6)	97.5(2)
O(2)-Dy(1)-O(5)#1	95.3(2)	O(2)-Dy(2)-O(4)	82.7(3)	O(5)-Dy(2)-N(4)	124.3(3)
O(2)-Dy(1)-O(6)	65.5(2)	O(2)-Dy(2)-O(5)	94.3(2)	O(5)-Dy(2)-N(5)	61.4(3)
O(2)-Dy(1)-N(1)	123.7(3)	O(2)-Dy(2)-O(6)	66.5(2)	O(6)-Dy(2)-N(4)	79.8(3)
O(2)-Dy(1)-N(2)	60.8(2)	O(2)-Dy(2)-N(4)	131.9(3)	O(6)-Dy(2)-N(5)	81.5(3)
O(3)#1-Dy(1)-O(5)#1	66.0(2)	O(2)-Dy(2)-N(5)	137.2(3)	N(4)-Dy(2)-N(5)	63.2(3)
O(3)#1-Dy(1)-O(6)	130.6(2)	O(3)-Dy(2)-O(4)	100.4(2)	Dy(1)-O(2)-Dy(2)	109.7(2)
O(3)#1-Dy(1)-N(1)	81.1(2)	O(3)-Dy(2)-O(5)	65.2(2)	Dy(2)-O(6)-Dy(1)	114.5(3)
O(3)#1-Dy(1)-N(2)	82.0(2)	O(3)-Dy(2)-O(6)	130.1(2)	Dy(1)#1-O(3)-Dy(2)	114.9(3)
O(5)#1-Dy(1)-N(1)	132.8(3)	O(3)-Dy(2)-N(4)	149.4(3)	Dy(1)-Dy(2)-Dy(1)#1	85.038(14)
#1 -x, y, -z+3/2					

Compound **5**

Dy(1)-O(1)	2.333(6)	Dy(2)-O(13)	2.288(6)	Dy(3)-N(8)	2.519(7)
Dy(1)-O(2)	2.351(6)	Dy(2)-O(17)	2.467(6)	Dy(4)-O(3)#1	2.301(6)
Dy(1)-O(4)	2.304(5)	Dy(2)-N(4)	2.472(7)	Dy(4)-O(7)	2.375(5)
Dy(1)-O(14)	2.285(5)	Dy(2)-N(5)	2.487(7)	Dy(4)-O(10)	2.384(6)
Dy(1)-O(15)	2.481(6)	Dy(1)-Dy(2)	3.7303(6)	Dy(4)-O(11)	2.330(6)
Dy(1)-O(16)	2.414(6)	Dy(3)-O(7)	2.345(6)	Dy(4)-O(18)	2.345(6)
Dy(1)-N(1)	2.455(6)	Dy(3)-O(8)	2.363(6)	Dy(4)-O(22)	2.442(7)
Dy(1)-N(2)	2.511(7)	Dy(3)-O(10)	2.315(5)	Dy(4)-N(10)	2.459(7)
Dy(2)-O(1)	2.446(5)	Dy(3)-O(19)	2.263(6)	Dy(4)-N(11)	2.507(7)
Dy(2)-O(4)	2.362(6)	Dy(3)-O(20)	2.447(6)	Dy(3)-Dy(4)	3.7494(6)
Dy(2)-O(5)	2.325(6)	Dy(3)-O(21)	2.420(6)		
Dy(2)-O(9)	2.262(5)	Dy(3)-N(7)	2.459(7)		
O(1)-Dy(1)-O(4)	75.22(19)	O(4)-Dy(2)-N(5)	128.8(2)	O(7)-Dy(4)-O(11)	93.8(2)
O(1)-Dy(1)-O(2)	165.45(18)	O(5)-Dy(2)-N(5)	63.5(2)	O(10)-Dy(4)-O(11)	164.26(19)
O(2)-Dy(1)-O(4)	90.34(19)	N(4)-Dy(2)-N(5)	63.2(2)	O(3)#1-Dy(4)-N(10)	75.6(2)
O(1)-Dy(1)-N(1)	67.1(2)	O(7)-Dy(3)-O(8)	160.22(18)	O(7)-Dy(4)-N(10)	131.3(2)
O(2)-Dy(1)-N(1)	126.4(2)	O(7)-Dy(3)-O(10)	72.62(19)	O(10)-Dy(4)-N(10)	66.1(2)
O(4)-Dy(1)-N(1)	139.8(2)	O(8)-Dy(3)-O(10)	90.91(19)	O(11)-Dy(4)-N(10)	125.9(2)
O(1)-Dy(1)-N(2)	129.6(2)	O(7)-Dy(3)-N(7)	66.9(2)	O(3)#1-Dy(4)-N(11)	76.0(2)
O(2)-Dy(1)-N(2)	63.6(2)	O(8)-Dy(3)-N(7)	125.8(2)	O(7)-Dy(4)-N(11)	144.4(2)
O(4)-Dy(1)-N(2)	149.4(2)	O(10)-Dy(3)-N(7)	138.1(2)	O(10)-Dy(4)-N(11)	128.5(2)
N(1)-Dy(1)-N(2)	62.8(2)	O(7)-Dy(3)-N(8)	128.0(2)	O(11)-Dy(4)-N(11)	62.6(2)
O(1)-Dy(2)-O(4)	72.07(18)	O(8)-Dy(3)-N(8)	63.5(2)	N(10)-Dy(4)-N(11)	63.3(2)
O(1)-Dy(2)-O(5)	92.17(19)	O(10)-Dy(3)-N(8)	149.9(2)	Dy(1)-O(1)-Dy(2)	102.61(19)
O(4)-Dy(2)-O(5)	164.19(19)	N(7)-Dy(3)-N(8)	62.4(2)	Dy(1)-O(4)-Dy(2)	106.2(2)
O(1)-Dy(2)-N(4)	130.8(2)	O(3)#1-Dy(4)-O(7)	135.1(2)	Dy(3)-O(7)-Dy(4)	105.2(2)
O(4)-Dy(2)-N(4)	66.5(2)	O(3)#1-Dy(4)-O(10)	100.3(2)	Dy(3)-O(10)-Dy(4)	105.9(2)
O(5)-Dy(2)-N(4)	126.6(2)	O(3)#1-Dy(4)-O(11)	93.1(2)		
O(1)-Dy(2)-N(5)	140.9(2)	O(7)-Dy(4)-O(10)	70.88(18)		
#1 x-1, y-1, z					

Table S3 Results of continuous shape measures analysis for the eight-coordinated Dy^{III} ions in **1**, **2**, **4** and **5**.

	TDD-8	BTPR-8	JSD-8
Dy (**1**)	3.755	3.783	3.514
Dy1 (**2**)	2.676	3.331	4.009
Dy1 (**4**)	3.409	4.129	4.003
Dy2 (**4**)	3.466	4.112	4.103
Dy1 (**5**)	3.183	3.254	5.475
Dy2 (**5**)	2.435	2.764	2.591
Dy3 (**5**)	3.213	3.070	5.065
Dy4 (**5**)	2.806	3.583	3.447

SAPR-8 Square antiprism (D_{4d}); TDD-8 Triangular dodecahedron (D_{2d}); BTPR-8 Biaugmented trigonal prism (C_{2v}); JSD-8 Snub diphenoid J84 (D_{2d})

Table S4 Results of continuous shape measures analysis for the nine-coordinated Dy^{III} ions in complex **3**.

	CSAPR-9	**TCTPR-9**	**MFF-9**
Dy1 (**3**)	2.203	2.648	**1.210**

CSAPR-9 Spherical capped square antiprism (C_{4v}); TCTPR-9 Spherical tricapped trigonal prism (D_{3h}); MFF-9 Muffin (C_s)

Table S5 Relaxation fitting parameters from least-squares fitting of $\chi(\omega)$ data in complex **3**.

T / K	χ_T / $cm^3\ mol^{-1}$	χ_S / $cm^3\ mol^{-1}$	α
1.9	23.63	0.46	0.081
2.2	20.40	0.39	0.084
2.5	17.30	0.40	0.069
2.8	15.11	0.40	0.059
3.1	13.38	0.42	0.053
3.4	11.98	0.38	0.049
3.7	10.81	0.36	0.045
4.0	9.85	0.33	0.041
4.3	9.04	0.36	0.037
4.5	8.56	0.39	0.028
4.8	8.14	0.37	0.027
5.0	7.57	0.41	0.022
5.5	6.76	0.40	0.019
6.0	6.11	0.44	0.023
6.5	5.56	0.29	0.025

Table S6 Computed energy levels (the ground state is set at zero), component values of the Lande factor *g* and wavefunction composition for each M_J state of the ground-state multiplet for Dy of complex **2**.

KD	Energy (cm^{-1})	g_X	g_Y	g_Z	Wavefunction composition*
1	0.0	0.02	0.06	19.40	0.93 |±15/2>
2	99.0	0.37	0.65	17.81	0.27 |±5/2> + 0.25 |±3/2> + 0.19 |±7/2> + 0.14 |±1/2>
3	135.2	0.13	0.92	15.58	0.81 |±13/2>
4	236.0	1.80	4.08	12.11	0.38 |±1/2>+ 0.32 |±11/2>+ 0.14 |±7/2>
5	280.4	2.23	5.92	12.20	0.33 |±11/2> + 0.29 |±1/2> + 0.17 |±5/2> + 0.10 |±3/2>
6	322.5	1.01	2.85	11.02	0.27 |±9/2> + 0.27 |±3/2> + 0.20 |±11/2>
7	408.3	1.15	2.48	13.91	0.35 |±9/2> + 0.21 |±3/2> + 0.17 |±7/2> + 0.15 |±5/2>
8	474.4	0.50	1.20	17.53	0.37 |±7/2> + 0.35 |±5/2> + 0.10 |±9/2>

*Only the contributions ≥ 10% are given.

Table S7 Computed energy levels (the ground state is set at zero), component values of the Lande factor *g* and wavefunction composition for each M_J state of the ground-state multiplet for Dy of complex **3**.

KD	Energy (cm-1)	g_X	g_Y	g_Z	Wavefunction composition*
1	0.0	0.02	0.03	19.47	0.94 |±15/2>
2	64.6	0.15	0.23	17.53	0.47 |±13/2> + 0.25 |±11/2> + 0.21 |±9/2>
3	126.5	0.09	0.21	16.94	0.31 |±7/2> + 0.26 |±5/2> + 0.16 |±3/2> + 0.10 |±11/2> + 0.10 |±1/2>
4	186.2	2.18	4.65	10.87	0.26 |±3/2>+ 0.20 |±13/2>+ 0.17 |±5/2> + 0.13 |±1/2>
5	229.6	8.64	7.14	0.15	0.28 |±1/2> + 0.21 |±13/2> + 0.21 |±9/2> + 0.12 |±3/2>
6	289.9	0.88	3.67	12.30	0.25 |±9/2> + 0.19 |±5/2> + 0.16 |±1/2> + 0.15 |±7/2> + 0.14 |±11/2>
7	307.0	2.81	5.07	11.60	0.37 |±11/2> + 0.26 |±7/2> + 0.15 |±9/2>
8	384.3	0.23	0.31	18.03	0.36 |±3/2> + 0.27 |±1/2> + 0.26 |±5/2>

* Only the contributions ≥ 10% are given.

Table S8 Computed energy levels (the ground state is set at zero), component values of the Lande factor *g* and wavefunction composition for each M_J state of the ground-state multiplet for Dy of complex **6**.

KD	Energy (cm^{-1})	g_X	g_Y	g_Z	Wavefunction composition*
1	0.0	0.01	0.02	19.62	0.96 |±15/2>
2	167.7	0.11	0.16	16.72	0.88 |±13/2>
3	334.8	10.15	7.47	2.89	0.41 |±11/2> + 0.13 |±3/2> + 0.13 |±1/2> + 0.11 |±7/2> + 0.10 |±5/2>
4	396.2	7.49	5.33	2.61	0.38 |±11/2>+ 0.19 |±1/2>+ 0.14 |±3/2> + 0.14 |±5/2>
5	509.6	4.23	4.72	11.02	0.43 |±9/2> + 0.21 |±1/2> + 0.14 |±3/2> + 0.11 |±7/2>
6	604.8	0.24	0.61	17.38	0.30 |±5/2> + 0.28 |±7/2> + 0.17 |±3/2> + 0.13 |±9/2>
7	661.5	0.13	0.76	15.22	0.31 |±1/2> + 0.25 |±3/2> + 0.14 |±9/2> + 0.12 |±7/2> + 0.11 |±5/2>
8	715.7	0.23	0.60	16.65	0.32 |±5/2> + 0.31 |±7/2> + 0.16 |±3/2>+ 0.11 |±9/2>

* Only the contributions ≥ 10% are given.

Table S9 Computed energy levels (the ground state is set at zero), component values of the Lande factor *g* and wavefunction composition for each M_J state of the ground-state multiplet for Dy of complex **7**.

KD	Energy (cm-1)	gX	gY	gZ	Wavefunction composition*
1	0.0	0.01	0.01	19.83	0.99 |±15/2>
2	163.9	0.03	0.04	17.17	0.97 |±13/2>
3	349.6	0.30	0.35	14.22	0.92 |±11/2>
4	488.4	3.38	3.77	10.61	0.81 |±9/2>
5	565.6	2.31	5.80	11.04	0.49 |±7/2> + 0.18 |±5/2> + 0.16 |±1/2> + 0.11 |±3/2>
6	600.5	0.87	2.16	13.72	0.33 |±5/2> + 0.28 |±3/2> + 0.24 |±7/2>
7	730.3	0.30	0.59	18.52	0.30 |±1/2> + 0.28 |±5/2> + 0.25 |±3/2> + 0.15 |±7/2>
8	831.9	0.14	0.38	19.44	0.37 |±1/2> + 0.34 |±3/2> + 0.20 |±5/2>

* Only the contributions ≥ 10% are given.

Table S10 Computed energy levels (the ground state is set at zero), component values of the Lande factor g and wavefunction composition for each M_J state of the ground-state multiplet for Dy of complex **8**.

KD	Energy (cm-1)	g_X	g_Y	g_Z	Wavefunction composition*
1	0.0	0.03	0.05	19.28	0.90 |±15/2>
2	139.8	0.12	0.21	16.35	0.87 |±13/2>
3	222.5	1.02	1.19	15.61	0.33 |±1/2> + 0.29 |±3/2> + 0.15 |±5/2>
4	252.5	2.76	6.63	10.98	0.33 |±11/2>+ 0.20 |±7/2>+ 0.18 |±5/2> + 0.10 |±9/2>
5	298.1	0.24	3.02	9.03	0.32 |±1/2> + 0.24 |±9/2> + 0.17 |±11/2> + 0.10 |±5/2>
6	324.9	2.20	2.90	12.42	0.25 |±7/2> + 0.21 |±11/2> + 0.18 |±3/2> + 0.16 |±9/2> + 0.12 |±5/2>
7	394.3	1.23	1.71	13.86	0.27 |±9/2> + 0.20 |±3/2> + 0.18 |±5/2> + 0.13 |±7/2> + 0.12 |±1/2>
8	442.5	0.85	3.42	16.30	0.27 |±7/2> + 0.26 |±5/2> + 0.17 |±3/2>+ 0.16 |±1/2> + 0.11 |±9/2>

*Only the contributions ≥ 10% are given.

Table S11 Relative energy and main component of the g-tensor (g_z) of the exchange KDs considering only dipolar interactions (J_{dip}) and with fitted exchange terms ($J_{dip} + J_{ex}$).

	Exchange KD	J^{dip} E / cm^{-1}	J^{dip} g_z	$J^{dip}+J^{ex}$ E / cm^{-1}	$J^{dip}+J^{ex}$ g_z
Complex 2	**1**	0.00	38.8	0.00	0
	2	1.89	0.0	0.52	38.8
Complex 3	**1**	0.00	38.9	0.00	38.9
	2	2.16	0.0	1.58	0.0
Complex 6	**1**	0.00	39.3	0.00	39.3
	2	2.38	0.0	1.21	0.0
Complex 7	**1**	0.00	39.7	0.00	39.7
	2	2.75	0.0	1.44	0.0
Complex 8	**1**	0.00	38.6	0.00	0.0
	2	2.01	0.0	0.14	38.6

References

[1] Aquilante, F.; Autschbach, J.; Carlson, R. K.; Chibotaru, L. F.; Delcey, M. G.; De Vico, L.; Galván, I. F.; Ferré, N.; Frutos, L. M.; Gagliardi, L.; Garavelli, M.; Giussani, A.; Hoyer, C. E.; Manni, G. L.; Lischka, H.; Ma, D. X.; Malmqvist, P.; Müller, T.; Nenov, A.; Olivucci, M.; Pedersen, T. B.; Peng, D. L.; Plasser, F.; Pritchard, B.; Reiher, M.; Rivalta, I.; Schapiro, I.; Segarra-Martí, J.; Stenrup, M.; Truhlar, D. G.; Ungur, L.; Valentini, A.; Vancoillie, S.; Veryazov, V.; Vysotskiy, V. P.; Weingart, O.; Zapata, F.; Lindh, R. Molcas 8: New Capabilities for Multiconfigurational Quantum Chemical Calculations Across the Periodic Table. *J. Comput. Chem*. **2016**, *37*, 506-541.

[2] Roos, B. O.; Taylor, P. R.; Siegbahn, P. E. M. A Complete Active Space SCF Method (CASSCF) Using a Density Matrix Formulated Super-CI Approach. *Chem. Phys.* **1980**, *48*, 157-173.

[3] Malmqvist, P.Å.; Roos, B.O.; Schimmel pfennig, B. The Restricted Active Space (RAS) State Interaction Approach with Spin-Orbit Coupling. *Chem. Phys. Lett.* **2002**, *357*, 230-240.

[4] Malmqvist, P.-Å.; Roos, B.O. The CASSCF State Interaction Method. *Chem. Phys. Lett.* **1989**, *155*, 189-194.

[5] Chibotaru, L.F.; Ungur, L. *Ab Initio* Calculation of Anisotropic Magnetic Properties of Complexes. I. Unique Definition of Pseudo spin Hamiltonians and Their Derivation. *J. Chem. Phys.* **2012**, *137*, 064112.
[6] Lines, M. E. Orbital angular momentum in the theory of paramagnetic clusters. *J. Chem. Phys.* **1971**, *55*, 2977-2984.
[7] Chibotaru, L.; Ungur, L.; Soncini, A. The Origin of Nonmagnetic Kramers Doublets in the Ground State of Dysprosium Triangles: Evidence for a Toroidal Magnetic Moment. *Angew. Chem., Int. Ed.* **2008**, *47*, 4126-4129.
[8] Aquilante, F.; Pedersen, T. B.; Lindh, R. Low-cost evaluation of the exchange Fock matrix from Cholesky and density fitting representations of the electron repulsion integrals. *J. Chem. Phys.* **2007**, *126*, 194106.
[9] Roos, B. O.; Lindh, R.; Malmqvist, P. A.; Veryazov, V.; Widmark, P. O. Main Group Atoms and Dimers Studied with A New Relativistic ANO Basis Set. *J. Phys. Chem.A.* **2004**, *108*, 2851-2858.
[10] Roos, B. O.; Lindh, R.; Malmqvist, P.; Veryazov, V.; Widmark, P. O.; Borin, A. C. New Relativistic Atomic Natural Orbital Basis Sets for Lanthanide Atoms with Applications to the Ce Diatom and LuF_3. *J. Phys. Chem. A.* **2008**, *112*, 11431-11435.
[11] Gagliardi, L.; Lindh, R.; Karlström, G. Local properties of quantum chemical systems: The LoProp approach. *J. Chem. Phys.* **2004**, *121*, 4494-4500.
[12] The CAMMEL code is available under GNU General Public License v3.0 and can be downloaded at https://github.com/rmarchal1/CAMMEL.
[13] Zhang, K.; Montigaud, V.; Cador, O.; Li, G.-P.; Le Guennic, B.; Tang, J.-K.; Wang, Y.-Y. Tuning the Magnetic Interactions in $Dy(III)_4$ Single-Molecule Magnets. *Inorg. Chem.* **2018**, 57, 8550-8557.
[14] Huang, G.; Fernandez-Garcia, G.; Badiane, I.; Camarra, M.; Freslon, S.; Guillou, O.; Daiguebonne, C.; Totti, F.; Cador, O.; Guizouarn, T.; Le Guennic, B.; Bernot, K. Magnetic Slow Relaxation in a Metal-Organic Framework Made of Chains of Ferro-magnetically Coupled Single-Molecule Magnets. *Chem. Eur. J.* **2018**, *24*, 6983-6991.